

# Trusting What You Cannot See: Auditable Fine-Tuning and Inference for Proprietary AI

Heng Jin  
*Virginia Tech*

Chaoyu Zhang  
*Virginia Tech*

Hexuan Yu  
*Virginia Tech*

Shanghao Shi  
*Washington University in St. Louis*

Ning Zhang  
*Washington University in St. Louis*

Y. Thomas Hou  
*Virginia Tech*

Wenjing Lou  
*Virginia Tech*

## Abstract

Cloud-based infrastructures have become the dominant platform for deploying large models, particularly large language models (LLMs). Fine-tuning and inference are increasingly delegated to cloud providers for simplified deployment and access to proprietary models, yet this creates a fundamental trust gap: although cryptographic and TEE-based verification exist, the scale of modern LLMs renders them prohibitive, leaving clients unable to practically audit these processes. This lack of transparency creates concrete security risks that can silently compromise service integrity.

We present AFTUNE, an auditable and verifiable framework that ensures the computation integrity of cloud-based fine-tuning and inference. AFTUNE incorporates a lightweight recording and spot-check mechanism that produces verifiable traces of execution. These traces enable clients to later audit whether the training and inference processes followed the agreed configurations. Our evaluation shows that AFTUNE imposes practical computation overhead while enabling selective and efficient verification, demonstrating that trustworthy model services are achievable in today’s cloud environments.

## 1 Introduction

Cloud-based infrastructures have become the dominant platform for deploying and customizing modern AI models [5, 9–11, 28, 34]. Infrastructure providers now host LLMs and provide managed APIs for fine-tuning, inference, and Model-as-a-Service deployments. For instance, OpenAI [28] offers GPT fine-tuning and hosted inference through its API, where clients submit data and access tuned models exclusively via API endpoints. Hundreds of thousands of models have been fine-tuned using OpenAI’s service [27]. As models grow ever larger, even for open-source models, enterprises are increasingly inclined to use the cloud to host fine-tuning and inference rather than maintaining local infrastructure.

However, this division of responsibility creates a funda-

mental visibility gap. Clients provide data and configurations but cannot independently verify whether providers execute fine-tuning and inference as contracted, and lack evidence linking delivered models or inference outputs to actual internal computation. Untrusted providers may downgrade the service or embed biases or even backdoors into the model. We outline some possible attacks in Appendix A, with attackers’ objectives and examples. At the same time, service providers lack the means to prove that they executed fine-tuning and inference as contracted, especially when they cannot provide model weights to the client (e.g., under API-only or proprietary-model deployments).

For proprietary models such as GPT and Gemini, model parameters must remain confidential, preventing clients from directly inspecting models to verify execution. This confidentiality requirement necessitates that both fine-tuning and inference be performed in the cloud. Thus, protecting only one process is insufficient: even if a service provider faithfully executes fine-tuning, they may engage in unexpected behavior during inference, and vice versa. This necessitates a unified verification framework that protects both processes.

**Existing literature and challenges on verifying fine-tuning and inference of LLM.** Verifiable computation in cloud environments has been a long-standing research topic. Most prior works aiming to enable verification without exposing details fall into two categories: zero-knowledge proof (ZKP) based approaches and trusted execution environment (TEE) based approaches. However, the increasing scale of modern large models introduces new challenges that existing approaches fail to address, due to the enormous memory occupation and computational requirements of these models.

ZKP-based approaches [3, 17, 23, 30, 38, 43] provide mathematical integrity for computations but incur prohibitive overhead due to the complexity of generating proofs for large-scale neural network operations. For example, state-of-the-art ZKP systems for model inference [30, 38] incur commitment overheads that are on the order of thousands times slower than standard plaintext execution (e.g., up to 15 minutes of overhead for a single-token inference of a 13B model [38]). [23]

applies ZKP to LLMs training but only supports LoRA (i.e., only a small portion of parameters can be trained) due to the overhead issue. For TEE-based approaches, [37, 40] run the inference pipeline within TEEs, and [13, 26, 31] run the whole pipeline within TEEs. Whether using TEEs on CPUs, GPUs, or NPUs, those approaches require the TEE to hold the entire model.

**Our work.** Given that ZKP-based approaches introduce unavoidable computational overhead, we adopt the TEE-based paradigm. However, to make TEE-based verification practical for large language models, the fundamental challenges mentioned above must be resolved. We present AFTUNE, a framework that enables verifiable integrity for cloud-based fine-tuning and inference while aiming to address the following limitations of all types of TEEs:

*Challenge 1) Memory constraints:* Modern LLMs exceed the trusted memory available to a single TEE instance. Models are routinely too large for one enclave-capable device and must be deployed via sharding across multiple GPUs or nodes. Fine-tuning makes this worse. Unlike inference, training requires additional persistent state such as optimizer moments and variance, plus large transient working sets including activations, gradients, and batch buffers. The memory footprint during fine-tuning is fundamentally different from inference and typically much larger. Directly applying existing run-inside-TEE techniques to fine-tuning is therefore impractical, as fine-tuning exceeds both the computational resources of a single node and its working set capacity.

*Solution 1) Block decomposition with compositional verification:* We exploit a key structural property of neural computation. Within a contiguous region of layers and steps, all internal states are deterministic functions of the region’s boundary states and the model/optimizer state at step boundaries. This allows us to decompose execution into independently verifiable blocks along layer and step dimensions. We record only boundary states, such as activations and gradients at layer-block edges and parameters plus optimizer state at step-block boundaries. Each block can be replayed inside an attested TEE as an atomic unit. Adjacent blocks share boundary tensors. Enforcing boundary continuity makes these local checks compose into end-to-end verification without requiring the full model or trace to reside in trusted memory.

*Challenge 2) Cost of evidence generation and verification:* Verifying the provider introduces two unavoidable costs. The provider must produce binding evidence during normal execution by computing commitments over large boundary tensors. Since clients cannot access proprietary model weights, verification must be performed on the provider side inside a TEE. At LLM scale, both are expensive. Cryptographic hashing over millions of tensor elements can become a throughput bottleneck if done naively. Recomputation-based audits can be substantial when replaying long segments with strict determinism requirements. This creates a tension between integrity, which demands dense evidence and thorough checking, and

practicality, which requires near-baseline training/inference performance and bounded verification effort.

*Solution 2) map-reduce style hashing and sampling-based verification:* We address execution overhead by making commitments accelerator-friendly. Instead of sequentially hashing each large tensor, we partition tensors into chunks, hash chunks in parallel on the accelerator, and aggregate them into a single commitment. This reduces the impact on the baseline pipeline. We address verification overhead by sampling. The client verifies only a sampled subset of blocks, with randomness chosen by the verifier and hidden until audit time. This yields probabilistic detection guarantees and compounds deterrence over repeated audits. Because block checks are independent, audits can be parallelized across TEEs without consuming accelerator resources, allowing verification to scale while leaving accelerators available for primary workloads.

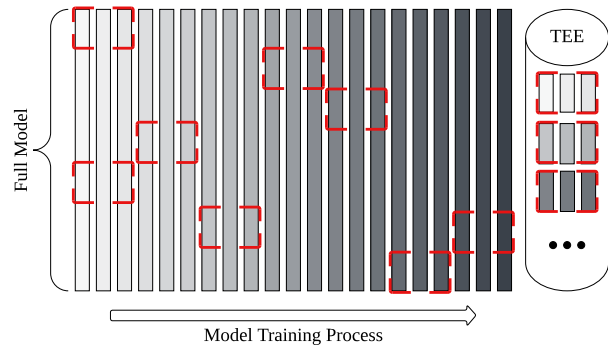


Figure 1: Each rectangle represents the full model at one training step. The red dashed border indicates blocks that will be independently verified, each of which contains only a portion of the training procedure.

The main contributions of this paper are:

- We propose AFTUNE, a verifiable framework for cloud-based fine-tuning and inference that decouples verification from the fine-tuning process by block-based evidence generation. This allows AFTUNE overcome the resource constraints in trusted container, allowing users to verify the fine-tuning process while preserving proprietary model parameters.
- We introduce a sampling-based verification strategy that provides probabilistic detection guarantees at practical costs, along with a map-reduce style hashing scheme for efficient commitment generation.
- We implemented AFTUNE and integrated it into CUDA-based training and inference pipelines. We evaluated our system on real TEE hardware with multiple open-source models across different model families and sizes, using both full fine-tuning and parameter-efficient fine-tuning,

demonstrating near-baseline performance and practical verification costs.

## 2 Related Work

Various approaches have been proposed to establish trust in cloud-based AI services, spanning behavioral testing, cryptographic verification, and hardware-based isolation.

Red-team evaluations can expose functional or safety issues in deployed models [16, 24], but only test known threat patterns and cannot verify whether fine-tuning followed the contracted procedure or whether the served model corresponds to the expected checkpoint. These approaches provide behavioral validation rather than process integrity guarantees.

Cryptographic approaches, particularly zero-knowledge proofs, offer strong integrity guarantees for computation [3, 17, 23, 30, 32, 38, 43]. As discussed in Section 1, existing ZK-based approaches incur prohibitive computational overhead, making them impractical for production deployment. Trusted execution environments provide hardware-enforced isolation that preserves code and data integrity even when the OS is compromised. Common TEEs include ARM TrustZone [4], Intel SGX [12], and RISC-V Keystone [21]. TEEs support remote attestation, allowing verifiers to cryptographically validate software state through hardware-signed measurements. Prior work has applied TEE-backed remote attestation to model execution [8, 13, 26, 31, 37, 40, 48, 49]. However, as discussed in Section 1, running entire fine-tuning or inference pipelines inside TEEs is impractical for large models due to memory constraints and performance overhead.

Some recent attempts address verification through indirect methods, but their scope remains limited. SVIP [39] requires service providers to return hidden states and verifies model identity through designed tasks, but only addresses the problem of providers using cheaper models during inference. VTUNE [47] inserts backdoors into training datasets and detects their presence afterward, but only catches cases where the provider completely skips fine-tuning and uses the base model.

## 3 Threat Model

We assume the client supplies the training dataset and specifies fine-tuning hyperparameters, while the service provider operates the training infrastructure. We consider proprietary model fine-tuning, where the client cannot access model parameters at any stage and must rely entirely on the provider for both training and inference.

We assume the service provider publicly releases the hash commitment of the base model as the initial trusted checkpoint for verifiable fine-tuning. We assume the cloud platform provides TEE-enabled infrastructure supporting remote attestation, allowing the client to verify TEE measurements and

establish secure channels to provision verification workloads to attested enclaves. Due to TEE memory constraints, we do not assume that the entire model can be loaded into the TEE at once for either training or inference. We do assume, however, that no single parameter tensor (i.e., individual weight array that is the unit of computation in the model) exceeds the TEE’s memory capacity. In our TEE setting, we have not observed any existing model, regardless of parameter count, that fails to satisfy this requirement.

We assume the attacker is a misbehaving or compromised cloud provider who aims to manipulate training or inference processes while evading detection. The adversary may control all software and infrastructure outside the TEE, fully understand AFTUNE’s design and verification mechanisms, and perform training manipulation or inference attacks as detailed in Appendix A. While potential attacks against TEEs or cryptographic hash functions exist, addressing or mitigating such attacks is outside the scope of this work.

We assume the defender is the client of the cloud service provider. The objective of AFTUNE is to enable the client to verify that training adhered to the contracted dataset, model, and hyperparameters, and that inference outputs are genuine predictions from the verified model, without requiring access to model parameters.

## 4 Overview

TEEs have seen significant growth over the past decade, with GPU TEEs now emerging. However, due to the size of modern LMs, it remains impractical to train any practical LM on a single node, let alone within the TEE on that node. TEEs inherently limit computational capability due to security constraints [22]. Furthermore, modern LM training uses heterogeneous accelerators such as GPUs, NPUs, FPGAs, and ASICs to tackle performance challenges [14, 19, 36, 41, 45]. While CPU TEEs are widely available, TEE support for these accelerators remains inconsistent, and extending TEE-based verification across such distributed heterogeneous fabrics presents unique technical and deployment challenges. In this work, we take a different approach. Rather than requiring TEEs on all components of the training infrastructure, we anchor trust in widely available CPU TEEs and extend this trust to the fine-tuning process without requiring systematic changes to the complex training infrastructure.

Our approach relies on the practical availability of TEE infrastructure, supported by the growing adoption of confidential computing across major cloud platforms such as Google Cloud [1] and AWS [2]. We leverage remote TEE enclaves on the provider side. Clients specify verification tasks that execute inside the TEE, where the enclave accesses model parameters, verifies computations, and returns only verification results to the client. This design ensures model parameters never leave the secure enclave while still providing clients with attestation of correct execution. Instead

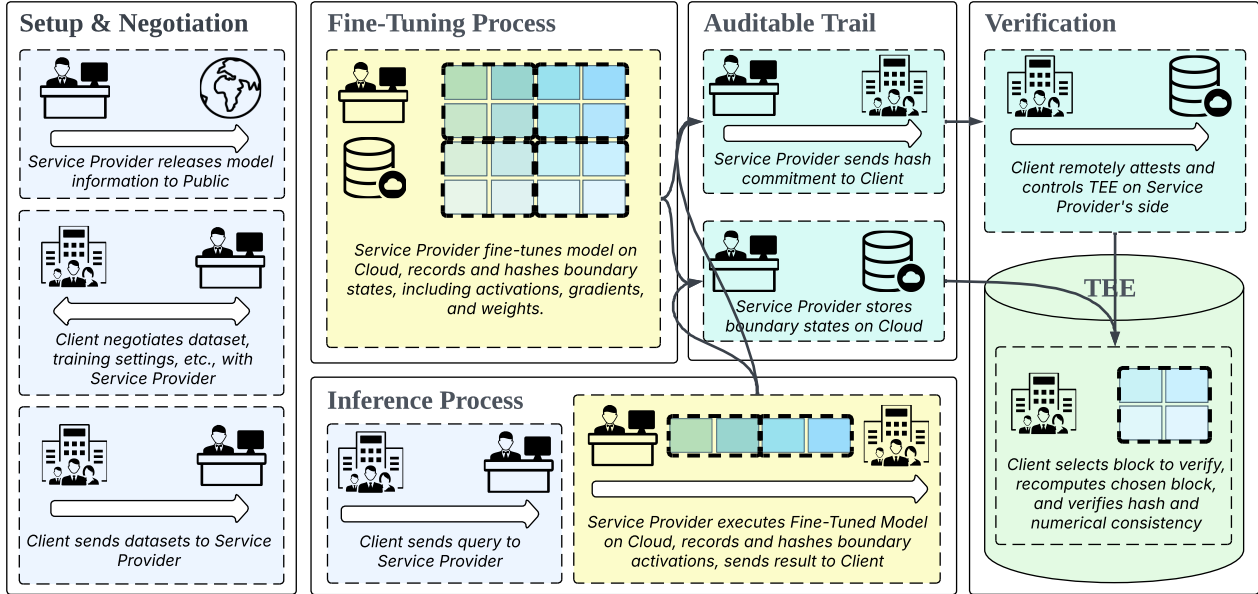


Figure 2: **AFTUNE workflow overview.** The system operates through setup and negotiation, fine-tuning, and inference phases. During execution, the provider commits boundary state hashes to the client and stores boundary states in cloud storage. Clients can verify training or inference computations on-demand through TEE-based selective recomputation of sampled regions.

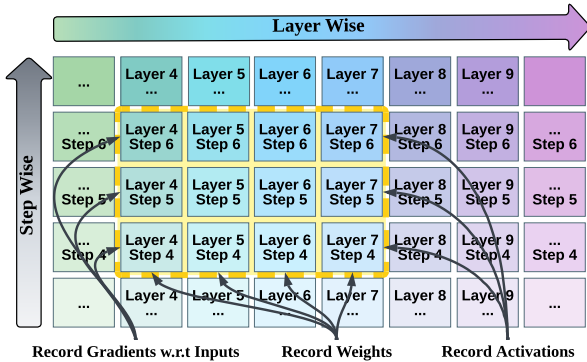


Figure 3: Two-dimensional block structure organizing the training procedure. The dashed border shows a single block spanning 4 layers and 3 steps. AFTUNE records only boundary states: activations and gradients at layer block edges, parameters and optimizer states at step block boundaries. Each block serves as an atomic, independently verifiable unit.

of executing the entire training process inside a TEE, AFTUNE decouples training execution from verification. The key insight is that we do not need real-time protection of computations during training; instead, we generate cryptographic evidence during execution and verify correctness afterward. This allows the primary fine-tuning workload to run at full speed on standard accelerator infrastructure while recording cryptographic commitments, using TEEs only for lightweight

recomputation-based verification after execution completes. This design avoids the resource and performance constraints of full TEE encapsulation while still providing verifiability.

Figure 2 illustrates AFTUNE’s workflow. During training and inference, AFTUNE records boundary states at strategic points and commits their hashes to the client, creating a cryptographic binding without requiring TEE involvement in the main computation path. The committed hashes may be signed by the service provider’s private key to prove authenticity. Verification occurs on-demand after execution completes. The client selects a target region (layer and step ranges for training, or layer ranges for inference) to verify, which we later refer to as a block. A TEE instance recomputes only the selected block, then validates the recorded states through hash matching and verifies computational correctness by comparing recomputed values against recorded states within floating-point tolerance. Because recomputation targets small regions rather than full execution traces, TEE resource constraints are satisfied.

To balance verification granularity with storage and computational efficiency, AFTUNE organizes the training procedure into a two-dimensional grid of blocks, as shown in Figure 3. Specifically, AFTUNE groups consecutive layers into layer blocks and consecutive training steps into step blocks, creating a grid where each cell represents their intersection. Hashes and intermediate states are recorded only at block boundaries, significantly reducing hash computations and stored audit data compared to per-layer, per-step recording. Clients can verify any block independently, with recomputation cost scal-

ing proportionally to block size. Hash computation itself is parallelized through a map-reduce scheme that partitions each tensor into chunks, computes hashes in parallel on the accelerator, and aggregates them into a single commitment. Since each block’s commitment contains only hash values, the cost of transmitting and storing commitments is negligible.

Together, these mechanisms enable AFTUNE to provide end-to-end auditability without the prohibitive costs of full TEE encapsulation, transforming opaque cloud services into transparent, accountable fine-tuning and inference platforms.

While our design focuses on proprietary model fine-tuning, it also applies to open-source model scenarios where clients outsource training but may obtain final weights for offline verification and self-hosted inference. Access to weights makes verification strictly easier, so our framework naturally remains valid.

## 5 Design

### 5.1 Notation and Problem Formulation

We formalize the fine-tuning verification problem and establish notation used throughout this section. Consider a neural network model with  $L$  layers indexed by  $\{l_0, l_1, \dots, l_{L-1}\}$ . Training proceeds for  $T$  steps indexed by  $\{t_0, t_1, \dots, t_{T-1}\}$ . For each layer  $l$  and step  $t$ , we denote  $x_{l,t} \in \mathbb{R}^{d_l}$  and  $y_{l,t} \in \mathbb{R}^{d_l}$  as the input and output activations, respectively. The corresponding gradients are denoted  $\nabla x_{l,t} \in \mathbb{R}^{d_l}$  (input gradient) and  $\nabla y_{l,t} \in \mathbb{R}^{d_l}$  (output gradient). Each layer  $l$  has associated parameters  $\theta_{l,t} \in \mathbb{R}^{p_l}$  and optimizer state  $s_{l,t}$  (e.g., momentum and variance for AdamW) at step  $t$ . The complete model parameters at step  $t$  are  $\theta_t = \{\theta_{l,t}\}_{l=0}^{L-1}$  and optimizer states are  $s_t = \{s_{l,t}\}_{l=0}^{L-1}$ .

The forward pass at layer  $l$  and step  $t$  computes  $y_{l,t} = f_l(x_{l,t}; \theta_{l,t})$ . The backward pass computes  $\nabla x_{l,t} = \frac{\partial \mathcal{L}_t}{\partial x_{l,t}}$  and  $\nabla \theta_{l,t} = \frac{\partial \mathcal{L}_t}{\partial \theta_{l,t}}$  via backpropagation, where  $\mathcal{L}_t$  is the loss at step  $t$ . After each step, parameters are updated via an optimizer:  $\theta_{l,t+1}, s_{l,t+1} = \text{Update}(\theta_{l,t}, s_{l,t}, \nabla \theta_{l,t}, \eta)$  for each layer  $l$ , where  $\eta$  denotes hyperparameters such as learning rate.

**Training verification:** Given an initial model with parameters  $\theta_0$  whose cryptographic hash  $h_0 = H(\theta_0)$  is known and trusted, a training dataset  $\mathcal{D} = \{(\mathbf{x}_i, \mathbf{y}_i)\}_{i=1}^N$ , and a hyperparameter configuration  $\mathcal{H}$ , the client verifies that the provider’s claimed checkpoint  $\theta_T$  was produced by executing  $T$  training steps according to  $\mathcal{H}$  on dataset  $\mathcal{D}$ , starting from  $\theta_0$ . Furthermore, the client verifies that intermediate training states (activations, gradients) were computed correctly at each layer and step, and that no data poisoning, training degradation, or parameter tampering occurred.

**Inference verification:** Given a verified model with parameters  $\theta^*$  (whose hash has been established through commitment and verification), an input  $\mathbf{x}$ , and the provider’s claimed output  $\mathbf{y}$ , the client verifies that  $\mathbf{y}$  was produced by computing

the forward pass through all  $L$  layers with parameters  $\theta^*$  on input  $\mathbf{x}$ , and that no model substitution, output fabrication, or computation tampering occurred.

### 5.2 Two-Dimensional Block Structure

A naive approach to verifiable training would record activations and gradients at every layer for every training step, incurring prohibitive storage costs that scale as  $O(L \times T)$  for a model with  $L$  layers trained for  $T$  steps. For large models and long training runs, this quickly becomes impractical. Moreover, computing cryptographic commitments requires  $L \times T$  hash operations, introducing significant computational overhead. A similar problem exists for inference, where per-layer recording would scale linearly with model depth.

The key observation is that not all intermediate states need explicit storage. Given activations at layer  $l$  and model parameters, activations at layer  $l + 1$  can be deterministically recomputed via forward propagation. Similarly, given gradients at layer  $l + 1$ , gradients at layer  $l$  can be recomputed via backpropagation. This enables a selective recording strategy: save states only at strategic boundaries, and reconstruct missing states through recomputation during verification.

AFTUNE organizes the training procedure into a two-dimensional grid of blocks along the layer and step dimensions. Define the layer block size  $B_L$  and step block size  $B_S$ . The  $L$  layers are partitioned into  $\lceil L/B_L \rceil$  *layer blocks*:

$$\text{LB}_i = \{l_{i \cdot B_L}, l_{i \cdot B_L + 1}, \dots, l_{\min((i+1) \cdot B_L - 1, L-1)}\} \quad (1)$$

for  $i = 0, 1, \dots, \lceil L/B_L \rceil - 1$ . Similarly, the  $T$  training steps are partitioned into  $\lceil T/B_S \rceil$  *step blocks*:

$$\text{SB}_j = \{t_{j \cdot B_S}, t_{j \cdot B_S + 1}, \dots, t_{\min((j+1) \cdot B_S - 1, T-1)}\} \quad (2)$$

for  $j = 0, 1, \dots, \lceil T/B_S \rceil - 1$ . Each combination of a *layer block* and a *step block* defines a *block cell*:

$$\text{Block}_{i,j} = \text{LB}_i \times \text{SB}_j. \quad (3)$$

For each  $\text{Block}_{i,j}$ , we record boundary activations  $x_{i \cdot B_L, t}$  (input to first layer) and  $y_{(i+1) \cdot B_L - 1, t}$  (output from last layer) for all steps  $t \in \text{SB}_j$ . Similarly, we record the corresponding gradients  $\nabla x_{i \cdot B_L, t}$  and  $\nabla y_{(i+1) \cdot B_L - 1, t}$  for all  $t \in \text{SB}_j$ . Additionally, parameters  $\theta_{l,t}$  and optimizer states  $s_{l,t}$  for layers  $l \in \text{LB}_i$  are recorded at step block boundaries  $t = j \cdot B_S$  and  $t = (j + 1) \cdot B_S$ .

The correctness of this boundary-only recording strategy relies on the continuity property of neural network computation: the output of layer block  $\text{LB}_i$  serves as the input to layer block  $\text{LB}_{i+1}$ , formally  $y_{l_{\text{last}(i)}, t} = x_{l_{\text{first}(i+1)}, t}$  for all steps  $t$ . Similarly, during backpropagation, the input gradient to block  $\text{LB}_{i+1}$  equals the output gradient of block  $\text{LB}_i$ :  $\nabla x_{l_{\text{first}(i+1)}, t} = \nabla y_{l_{\text{last}(i)}, t}$ . This continuity ensures that boundary states for adjacent blocks chain together, enabling complete verification of the forward and backward passes across all

layers for any training step by recomputing within each block and validating boundary consistency.

Boundary continuity enables storage and computation deduplication. Since the output activation of block  $LB_i$  is identical to the input activation of block  $LB_{i+1}$ , we need only store this tensor once and compute its cryptographic hash once, despite it serving as a boundary for two adjacent blocks. The same principle holds for gradients during backpropagation, as shown in Figure 3. As a result, instead of storing and hashing  $2 \times \lceil L/B_L \rceil$  boundary states per step (an input and output for each block), we only store and hash  $\lceil L/B_L \rceil + 1$  boundaries (one between each pair of adjacent blocks, plus the initial input and final output). Further optimization through sparse checkpointing is discussed in Section 5.6.

### 5.3 Map-Reduce Hashing Scheme

To bind recorded boundary states to tamper-evident commitments, we compute cryptographic hashes over boundary tensors during training. Any tampering with stored states will produce a hash mismatch during verification, ensuring that the recorded execution is cryptographically bound to its commitments.

However, computing cryptographic hashes sequentially over large tensors (e.g., millions of elements) creates a performance bottleneck that would significantly degrade training throughput.

To address this, AFTUNE employs a map-reduce hash design optimized for accelerator (e.g., GPU) parallelism. The key idea is to partition each tensor into fixed-size chunks, compute hashes for all chunks in parallel on the accelerators, and then aggregate the chunk hashes into a single final hash.

For a tensor  $X \in \mathbb{R}^{d_1 \times d_2 \times \dots \times d_n}$  with  $N = \prod_{i=1}^n d_i$  elements, the hashing procedure operates as follows:

1. **Flatten:** Convert  $X$  to a one-dimensional array  $X_{\text{flat}} \in \mathbb{R}^N$ .
2. **Partition:** Divide  $X_{\text{flat}}$  into  $m = \lceil N/C \rceil$  fixed-size chunks, where  $C$  is the chunk size:

$$X_{\text{flat}} = [\text{chunk}_0 \| \text{chunk}_1 \| \dots \| \text{chunk}_{m-1}], \quad (4)$$

with  $\text{chunk}_k \in \mathbb{R}^C$  for  $k = 0, \dots, m-1$ .

3. **Parallel hash:** Compute hashes for all chunks in parallel on accelerators, where each chunk is assigned to a separate thread:

$$h_k = H(\text{chunk}_k) \quad \text{for } k = 0, 1, \dots, m-1, \quad (5)$$

where  $H$  is a cryptographic hash function such as BLAKE3 or SHA-256.

4. **Aggregate:** Compute the final hash on the CPU by hashing the concatenation of all chunk hashes:

$$H(X) = H(h_0 \| h_1 \| \dots \| h_{m-1}). \quad (6)$$

This design parallelizes the hash computation across accelerators by flattening the tensor and distributing chunks to independent threads, avoiding sequential processing. The aggregate step ensures that the final hash depends on all chunks and their ordering, such that any modification to  $X$  will produce a different hash value, enabling tamper detection.

Applying this hashing scheme to the boundary states defined in Section 5.2, for each  $\text{Block}_{i,j}$ , we compute and record:

$$\begin{aligned} \mathcal{R}_{i,j} = & \{ H(x_{i \cdot B_L, t}), H(y_{(i+1) \cdot B_L - 1, t}), \\ & H(\nabla x_{i \cdot B_L, t}), H(\nabla y_{(i+1) \cdot B_L - 1, t}) \}_{t \in \text{SB}_j} \\ & \cup \{ H(\theta_{l,j \cdot B_S}), H(s_{l,j \cdot B_S}), \\ & H(\theta_{l,(j+1) \cdot B_S}), H(s_{l,(j+1) \cdot B_S}) \}_{l \in \text{LB}_i}. \end{aligned} \quad (7)$$

These hashes form the tamper-evident audit trail that binds the recorded training execution to its commitments.

### 5.4 Recomputation-Based Verification Protocol

With the block structure and cryptographic hashes established, we now describe how clients verify training and inference integrity and correctness. The verification protocol employs recomputation: given model parameters and boundary states, the client re-executes the computation within the TEE and compares recomputed tensors against recorded hashes and values. Hash matching confirms data integrity; numerical matching within floating-point tolerance confirms computational correctness. Algorithm 1 in Appendix B presents the verification protocol for training block cell  $\text{Block}_{i,j}$ . For notation simplicity, we denote  $l_{\text{in}} = l_{i \cdot B_L}$  and  $l_{\text{out}} = l_{(i+1) \cdot B_L - 1}$  as the block’s input and output layers.

Hash matching confirms bitwise integrity: matching hashes indicate no tampering with recorded data. Numerical verification accounts for non-determinism in floating-point operations across hardware or software configurations. The relative  $L^2$  error is compared against a threshold  $\tau$  determined by the precision format (e.g., float32, bfloat16) and acceptable error bounds. This tolerance-based approach is essential for seamless integration: by accommodating legitimate floating-point variations, AFTUNE operates on standard infrastructure without requiring deterministic hardware, specialized frameworks, or modifications to existing ML pipelines. The effectiveness of verifying individual blocks may seem counterintuitive, especially considering that the hashes used for verification are computed by the service provider rather than the client. We provide a detailed explanation of why this approach is valid in Appendix C.

Importantly, block verification is inherently parallelizable: each block cell can be verified independently since it only depends on its boundary states. When verifying multiple blocks, clients can distribute the workload across multiple TEE instances, enabling scalable verification that grows linearly with

available TEE resources rather than requiring sequential processing of the entire training trace.

## 5.5 Inference Verification Protocol

Inference verification applies to both fine-tuned models (after training) and base models (when clients rely on the provider solely for inference). AFTUNE extends the verification protocol to inference workloads to prevent model substitution or output fabrication.

Inference verification follows the same block structure and verification strategy as training, with two differences. First, only forward passes are recorded and recomputed, as inference involves no backpropagation or parameter updates. Second, each inference request is treated as a single step ( $B_S = 1$ ). For each inference request with input  $\mathbf{x}$ , the provider records boundary activations  $x_{i \cdot B_L}$  and  $y_{(i+1) \cdot B_L - 1}$  for each layer block  $LB_j$ , along with their cryptographic hashes.

The client verifies an inference request by loading the select block into TEE memory and recomputing the forward pass. The recomputed activations and their hashes are compared against the recorded values using the same hash matching and numerical verification procedures described in Section 5.4. Any attempt to substitute the model or fabricate outputs will produce mismatches in the intermediate or final prediction, enabling detection. This ensures end-to-end auditability: clients can verify not only that training was executed correctly, but also that inference outputs are genuine predictions from the contracted model.

## 5.6 Storage Optimization via Sparse Checkpointing

The design presented so far assumes that model parameters and optimizer states are saved at every step block boundary. While this provides direct verification, it may impose significant storage costs for long training runs.

To address this, AFTUNE supports sparse checkpointing strategies that trade storage for verification-time recomputation. Missing checkpoints or activations can be reconstructed via recomputation from nearby stored states. This enables flexible storage-computation trade-offs tailored to different deployment scenarios.

For training verification, we introduce the checkpoint interval  $I_C$  to control the frequency of checkpointing along the step dimension. A checkpoint is saved at step block  $SB_j$  if and only if  $j \bmod I_C = 0$ . Each checkpoint comprises:

$$\text{Checkpoint}_t = \{\theta_t, s_t\}, \quad (8)$$

where  $t$  denotes the step at boundary  $j \cdot B_S$ . When  $I_C > 1$ , checkpoints are saved only at sparse intervals.

To verify a step block  $SB_j$  where no checkpoint was saved, the system locates the nearest prior checkpoint and recom-

putes intervening steps to reconstruct the model state at the beginning of  $SB_j$ . This recomputation executes forward passes, backward passes, and parameter updates for each intervening step. For the TEE to verify the reconstructed state via hash matching, recomputation must produce bitwise-identical results, requiring deterministic computation and consistent hardware/software configurations. The reconstructed state is then provided to the TEE for verification.

Sparse checkpointing assumes deterministic computation, but certain layers may contain operations lacking deterministic implementations on some accelerators. AFTUNE addresses this through flexible layer block design: non-deterministic layers can be isolated into separate layer blocks with  $I_C = 1$ , ensuring checkpoints are saved at every step boundary for these blocks. This selective strategy preserves verification correctness while enabling aggressive sparsity for deterministic layers.

With sparse checkpointing, the total storage cost for training becomes:

$$\text{Storage}_{\text{total}} = \frac{\lceil T/B_S \rceil}{I_C} \cdot (|\theta| + |s|) + (\lceil L/B_L \rceil + 1) \cdot T \cdot (|x| + |\nabla x|), \quad (9)$$

where  $|\theta|$  and  $|s|$  denote the sizes of parameters and optimizer states, and  $|x|$  and  $|\nabla x|$  denote the sizes of activations and gradients. The first term represents checkpoint storage (reduced by factor  $I_C$ ), and the second term represents activation and gradient storage at layer block boundaries.

For inference verification, where model parameters remain fixed, an alternative optimization applies an activation interval  $I_A$  along the layer dimension: boundary states for layer block  $LB_i$  are saved only if  $i \bmod I_A = 0$ . Missing activations are reconstructed by recomputing forward passes from adjacent recorded blocks.

## 5.7 Sampling-Based Spot-Check and Strategies

While clients can verify all blocks for maximum assurance, AFTUNE supports selective verification through sampling to reduce overhead while maintaining security guarantees. Sampling-based spot-checking has been successfully applied to verify the integrity of data stored on cloud [6, 35]. The key question is: how effective is probabilistic spot-checking for verifying computational processes?

Let  $N_{\text{blocks}} = \lceil L/B_L \rceil \times \lceil T/B_S \rceil$  denote the total number of block cells in the training or inference trace. If an adversary compromises  $k$  blocks and the client randomly verifies  $m$  blocks, the probability that the adversary evades detection is:

$$P_{\text{evade}} = \frac{\binom{N_{\text{blocks}} - k}{m}}{\binom{N_{\text{blocks}}}{m}} = \prod_{i=0}^{m-1} \frac{N_{\text{blocks}} - k - i}{N_{\text{blocks}} - i}. \quad (10)$$

The detection probability  $P_{\text{detect}} = 1 - P_{\text{evade}}$  can be approximated for small compromise ratios  $\rho = k/N_{\text{blocks}}$  as:

$$P_{\text{detect}} \approx 1 - (1 - \rho)^m \approx 1 - e^{-\rho m}. \quad (11)$$

Even modest verification efforts achieve substantial detection rates. For instance, if an adversary compromises 10% of blocks ( $k = 100$ ) and the client verifies only 1% ( $m = 10$ ) out of  $N_{\text{blocks}} = 1000$  total blocks, detection probability reaches  $P_{\text{detect}} \approx 65\%$ .

In addition, the single-round probabilities still understate the true deterrent power of spot-checking. The critical insight is that *the adversary must execute the attack without knowing which blocks or how many will later be verified*. This uncertainty forces the adversary to either avoid tampering entirely or risk detection, as any tampered block may be selected for verification. A single detection permanently destroys trust, which creates a powerful deterrent effect. When clients perform multiple independent verifications over time, the adversary’s evasion challenge compounds rapidly, driving cumulative detection probability toward certainty.

Unlike static data where all segments are homogeneous, computational processes exhibit distinct characteristics across different stages and components. Beyond uniform random sampling, clients can thus adapt strategies to their specific threat priorities. Most importantly, the attacker cannot know the client’s priority and verification strategy at the time of the attack. For backdoor and poisoning attacks, the client need only verify the input block at each training step. For training degradation attacks such as epoch reduction or directly using the base model, the existence of commitments already proves that training occurred. Randomly verifying a small number of blocks is sufficient to detect such attacks. For model substitution attacks, selecting one block across the layer dimension at each training step is enough. These input blocks constitute only a small fraction of all blocks, yet provide near-certainty detection for most such attacks. This strategic flexibility enables clients to achieve high detection rates with minimal verification cost tailored to specific threat models.

## 6 Evaluation

### 6.1 Experimental Setup

We evaluate AFTUNE across diverse model architectures to measure its overhead, storage efficiency, and verification accuracy. Some evaluations are available at Appendix D, E, F.

**Models.** We evaluate AFTUNE on both language and vision models to demonstrate its generality: Llama-3.1-8B [15] and Qwen2.5-14B [46] for language tasks, and DINOv2-Giant [29] and ViT-Large [42] for vision tasks. These models span different sizes, layer structures, and computational patterns.

**Datasets.** For LLM fine-tuning, we use MentalChat16K [44], a mental health conversational dataset. For vision models, we use ImageNet-1K [33] for image classification tasks.

**Baselines.** We compare AFTUNE against three baselines: (1) *Baseline*: standard training without verification, representing the performance upper bound; (2) *Full TEE*: the entire training process executes within a TEE, providing strong security but incurring significant overhead; (3) *Step TEE*: verification executes in TEE but checks one complete training step at a time across all layers, lacking AFTUNE’s flexible block-based granularity control. Note that due to memory constraints, Full TEE and Step TEE are only feasible for ViT-Large among our evaluated models. For other models, we execute on CPUs solely for overhead comparison.

**Configurations.** We vary block sizes  $B_L$  and  $B_S$ , hash functions, optimizers, and checkpoint intervals  $I_C$ . Default configuration uses  $B_L = 4$ ,  $B_S = 8$ , BLAKE3 hash function, SGD optimizer, batch size 16, bfloat16 precision, and  $I_C = 8$  unless otherwise stated. For hash computation, we use chunk size 4096 for Llama, Qwen, and DINOv2, and chunk size 1024 for ViT.

**Hardware and Environment.** Experiments run on NVIDIA RTX PRO 6000 GPUs with 96GB GPU memory and Intel Xeon Gold 5520+ CPUs for TEE verification with Intel SGX and TDX support. We implement the TEE verification component using Gramine [7, 20], a library OS that supports both Intel SGX and Intel TDX for hardware-backed attestation and isolation. The TEE memory is configured to 16GB, the maximum memory size supported by our platform.

### 6.2 System Overhead Analysis

Table 1 presents overhead comparisons across different models, methods, and block configurations. We report training time, storage cost per 2048 samples, block preparation time for verification, and TEE verification time per block cell. Block preparation time refers to the time required to reconstruct model states for a target block from the nearest prior checkpoint via recomputation (Section 5.6), measured at the worst-case recomputation distance for sparse checkpointing with interval  $I_C$ .

Larger models incur lower relative training overhead, as hash computation cost becomes proportionally smaller with increasing model size. Full TEE training remains impractical even for small models due to substantial overhead, and memory constraints prevent larger LLMs from loading. In contrast, AFTUNE achieves practical overhead through strategic block partitioning.

Block size configuration offers clear trade-offs between training overhead and storage cost: larger blocks reduce both metrics by decreasing the number of hash computations and boundary recordings. Compared to Step TEE verification, AFTUNE reduces storage costs by over half across all models.

Table 1: Comprehensive system overhead comparison per 2048 samples. Prep time is the time to prepare blocks for verification. Verify time is per block cell in TEE.

Model	Method	Block Size	Train Time (s)	Overhead	Storage (GB)	Prep Time (s)	Verify Time (s)
Qwen2.5-14B	Baseline	-	114.1	-	-	-	-
	Step TEE	-	199.2	75%	555.8	157.0	N/A <sup>1</sup>
	AFTUNE	$B_L = 2, B_S = 4$	150.1	32%	314.9	13.0	25.1
	AFTUNE	$B_L = 4, B_S = 8$	135.6	19%	213.5	20.3	58.0
	AFTUNE	$B_L = 4, B_S = 16$	129.8	14%	164.6	35.1	83.6
Llama-3.1-8B	Baseline	-	62.8	-	-	-	-
	Step TEE	-	114.8	83%	333.3	78.0	N/A <sup>1</sup>
	AFTUNE	$B_L = 2, B_S = 4$	85.7	36%	201.0	7.3	21.0
	AFTUNE	$B_L = 4, B_S = 8$	76.1	21%	146.2	15.1	48.2
	AFTUNE	$B_L = 4, B_S = 16$	74.0	18%	131.3	24.5	76.2
DINOv2-Giant	Baseline	-	24.1	-	-	-	-
	Step TEE <sup>2</sup>	-	87.6	263%	272.3	-	N/A <sup>1</sup>
	AFTUNE	$B_L = 4, B_S = 4$	44.1	83%	35.2	4.5	9.4
	AFTUNE	$B_L = 8, B_S = 8$	34.8	44%	19.1	10.4	25.6
	AFTUNE	$B_L = 16, B_S = 16$	30.1	25%	9.8	23.2	74.1
ViT-Large	Baseline	-	6.8	-	-	-	-
	Full TEE	-	210.7	3000%	-	-	-
	Step TEE	-	18.2	167%	9.6	3.1	19.7
	AFTUNE	$B_L = 8, B_S = 4$	11.6	71%	6.5	3.4	8.7
	AFTUNE	$B_L = 16, B_S = 8$	8.9	31%	2.9	4.6	15.3
AFTUNE	$B_L = 16, B_S = 16$	8.6	26%	2.3	7.6	21.7	

<sup>1</sup> Step TEE verification cannot be performed in TEE due to excessive memory consumption. CPU verification times are 331.3s (Qwen2.5-14B), 178.5s (Llama-3.1-8B), and 28.2s (DINOv2-Giant). TEE time is estimated at 1.5–2× CPU time.

<sup>2</sup> DINOv2-Giant contains modules with non-deterministic operations. AFTUNE isolates these layers into separate blocks with  $I_C = 1$ , while Step TEE cannot handle layer-wise separation and thus cannot use checkpointing.

Importantly, block verification can be performed in parallel without occupying GPU resources. The storage cost can be further managed, which we discuss in Section 8.1.

Figure 4 presents training overhead composition across different models using the second configuration from Table 1. Pie charts visualize time overhead (hash computation, I/O, and other AFTUNE operations) and storage overhead (activations, gradients, and parameters). Hash computation typically accounts for the majority of time overhead, as it requires GPU resources and stalls training until completion. Storage overhead composition varies by model architecture: some models are parameter-dominant while others have larger activation and gradient storage.

## 7 LoRA Fine-tuning

Low-Rank Adaptation (LoRA) [18] is a parameter-efficient fine-tuning method that freezes pre-trained weights and trains only low-rank adapter matrices. AFTUNE supports LoRA fine-tuning with the same verification guarantees as full fine-tuning.

**Performance and storage.** Table 2 shows the performance

and storage characteristics of LoRA fine-tuning with verification. We use rank  $r = 64$ , targeting query and value projection layers.

LoRA fine-tuning stores only small adapter matrices instead of full model parameters, while frozen base parameters are stored once and reloaded during verification. Activation and gradient storage remains identical to full fine-tuning, as forward and backward passes involve the same tensors. The verification protocol follows the same process as full fine-tuning.

Increasing  $I_C$  provides minimal benefit for LoRA, as parameter checkpoints are already small compared to activations and gradients. Training overhead is lower than full fine-tuning primarily because LoRA eliminates the cost of hashing large parameter tensors at each checkpoint.

### 7.1 Inference Verification

We measure inference latency overhead, storage cost, and verification time per inference request. Table 3 examines the impact of layer block size ( $B_L$ ) with  $I_A = 4$ .

Inference recording imposes modest latency overhead,

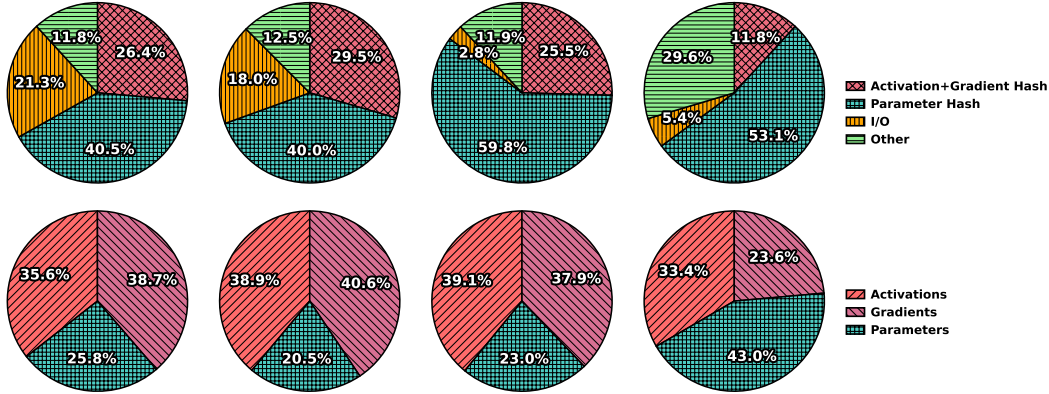


Figure 4: Training overhead composition across different models with the second configuration from Table 1. **Top row:** Time overhead proportions for Qwen2.5-14B, Llama-3.1-8B, DINOv2-Giant, ViT-Large (left to right), followed by legend showing hash computation, I/O, and other AFTUNE operations. **Bottom row:** Storage proportions for the same models, followed by legend showing activations, gradients, and parameters.

Table 2: LoRA fine-tuning with verification across 2048 samples. Rows with  $I_C = \text{“-”}$  are baselines.

Model	$I_C$	Training Time (s)	Overhead	Storage (GB)	Prep Time (s)	Verify Time (s)
	-	45.1	-	-	-	-
Llama-3.1-8B	1	52.8	17%	117.5	-	34.2
	8	52.5	16%	114.8	14.2	
	-	79.9	-	-	-	-
Qwen-2.5-14B	1	91.5	15%	160.0	-	39.9
	8	90.8	14%	158.6	17.6	

achieving as low as 10% in optimal configurations. Storage requirements per inference request are highly practical, typically ranging from 1-5 MB depending on model size and block configuration. Verification time is also acceptable, ranging from 5-15 seconds depending on model complexity, allowing clients to audit inference outputs efficiently.

## 7.2 Verification Correctness

We examine whether recomputation-based verification produces numerically accurate results for both inference and training.

**Training verification.** We measure the relative  $L^2$  error of recomputed parameters against expected values. Figure 5 reports the maximum layer-level parameter error for different layer block sizes ( $B_L$ ) and step block sizes ( $B_S$ ) using bfloat16 precision. These errors arise from floating-point computation differences between training and verification devices.

Numerical errors remain small across all configurations, well within acceptable tolerance for verification. The results reveal a clear error propagation trend: larger  $B_L$  and  $B_S$  lead to higher errors, as longer recomputation sequences accumulate more floating-point discrepancies. This reflects the fundamental trade-off between training overhead and verification accuracy: larger blocks reduce training overhead by

minimizing hash computation frequency but require longer recomputation chains that amplify numerical errors.

**Inference verification.** Figure 6 shows the relative  $L^2$  error between recomputed and recorded activations for inference verification across different models and layer block sizes, comparing bfloat16, float32, and float64 precision.

Similar to training verification, a larger  $B_L$  leads to higher errors due to longer recomputation sequences. However, bfloat16 precision produces errors too large for meaningful verification guarantees, making them easily exploitable by attackers, as we demonstrate in Section 7.3.1. In contrast, float32 precision reduces these errors by 3-4 orders of magnitude, providing reliable verification guarantees that effectively detect malicious manipulations.

## 7.3 Security Against Numerical Tolerance Exploitation

Both inference and training verification rely on numerical error thresholds to accommodate legitimate floating-point differences across devices. A security concern is whether adversaries could exploit these tolerances to inject malicious perturbations that remain below detection thresholds yet compromise model behavior. We evaluate this threat through two attack vectors: adversarial examples on activations (inference-

Table 3: Impact of layer block size on inference verification overhead with  $I_A = 4$ . Rows with  $B_L = \text{“-”}$  are baselines.

Model	$B_L$	Infer Time (ms)	Overhead	Storage (MB)	Verify Time (s)
Qwen2.5-14B	-	359	-	-	-
	1	409	14%	5.87	7.0
	2	392	9%	3.16	9.5
	4	387	8%	1.36	14.7
Llama-3.1-8B	-	341	-	-	-
	1	389	19%	3.75	6.3
	2	372	14%	2.09	8.3
	4	355	13%	0.84	12.5
DINOv2-Giant	-	267	-	-	-
	1	331	24%	8.60	4.6
	2	303	13%	4.82	4.9
	4	296	11%	2.56	5.3
ViT-Large	-	212	-	-	-
	1	266	25%	3.00	4.5
	2	241	14%	1.84	4.7
	4	241	14%	1.06	5.4

level) and parameter poisoning (training-level).

### 7.3.1 Adversarial Example Attacks on Activations

As established in Section 7.1, AFTUNE prevents providers from fabricating outputs by verifying recorded activations. However, could adversaries inject adversarial perturbations into intermediate activations that evade detection?

**Attack formulation.** We evaluate both untargeted and targeted attacks using Projected Gradient Descent (PGD) [25] with  $L_2$  norm constraints. In the untargeted setting, the adversary seeks to minimize the perturbation magnitude while flipping the model’s prediction:

$$\min_{\delta} \|\delta\|_2 \quad \text{s.t.} \quad \arg \max_i f(x + \delta)_i \neq \arg \max_i f(x)_i \quad (12)$$

In the targeted setting, the adversary forces the model to predict a specific target label  $t$ :

$$\min_{\delta} \|\delta\|_2 \quad \text{s.t.} \quad \arg \max_i f(x + \delta)_i = t \quad (13)$$

To maximize attack strength, we consider adversaries that inject perturbations at every block boundary activation throughout the model. For a model with  $B$  blocks, the adversary optimizes perturbations  $\{\delta_b\}_{b=1}^B$  at each block boundary to collectively minimize the  $L_2$  norm while achieving the attack objective.

**Evaluation.** We evaluate the attack with varying layer block sizes to understand how block granularity affects the perturbation budget required for successful attacks. Figure 8 summarizes the maximum and minimum  $L_2$  perturbation magnitudes across all blocks for both untargeted and targeted attacks.

Maximum perturbations occur predominantly at early layers while minimum perturbations concentrate at later layers,

as later layers require smaller perturbations due to shorter propagation paths to the output. As  $B_L$  increases, maximum perturbations decrease because recorded activations shift to later layers, while minimum perturbations increase due to fewer boundaries to exploit.

Comparing these perturbation magnitudes against numerical errors in Figure 6 reveals a critical vulnerability when using bfloat16 precision. In many configurations, adversarial perturbations fall within or near bfloat16’s recomputation error range, making it nearly impossible to establish an effective threshold that distinguishes malicious perturbations from legitimate numerical errors without triggering excessive false positives. This enables attacks that evade detection by exploiting the inherent numerical tolerance.

In contrast, float32’s numerical errors remain orders of magnitude smaller than even the minimum adversarial perturbations across all configurations. This separation provides a clear security margin for detection. Furthermore, float64 precision provides far more separation than necessary for verification, reducing numerical errors to negligible levels. Therefore, inference verification requires at least float32 precision. Importantly, both precision levels are supported by standard GPU hardware, preserving AFTUNE’s seamless integration with existing ML infrastructure.

### 7.3.2 Parameter Poisoning Attacks on Model Weights

Training verification records parameter hashes at block boundaries, subject to numerical recomputation errors. Could adversaries exploit these tolerances by injecting small parameter perturbations to compromise model behavior?

**Attack formulation.** Unlike adversarial example attacks, where the attack surface depends on  $B_L$ , parameter poisoning attacks can target any subset of model weights regardless of

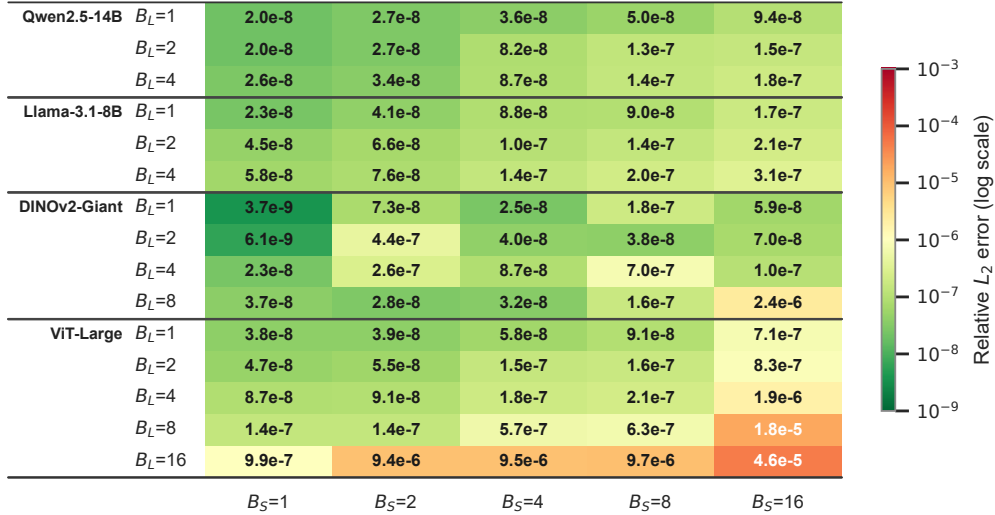


Figure 5: Training verification accuracy; parameter relative  $L_2$  error across layer block sizes and step block sizes.

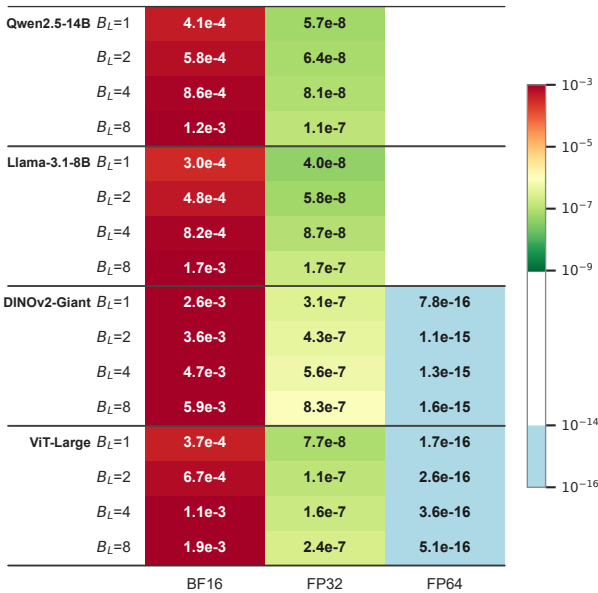


Figure 6: Inference verification accuracy; activation relative  $L_2$  error across layer block sizes and precision levels.

block structure. To maximize attack strength, we perturb all model parameters simultaneously, formulated as a constrained optimization that minimizes the  $L_2$  norm of perturbations  $\Delta\theta$  while achieving attack objectives.

For backdoor injection, we inject a trigger (a trigger word for LLMs or a trigger pattern for vision models) that causes

misclassification while preserving normal behavior:

$$\min_{\Delta\theta} \|\Delta\theta\|_2 \quad \text{s.t.} \quad \begin{cases} f_{\theta+\Delta\theta}(x_{\text{trigger}}) = y_{\text{target}} & \forall x_{\text{trigger}} \\ \mathcal{L}(f_{\theta+\Delta\theta}(x_{\text{clean}}), y_{\text{clean}}) \approx 0 & \forall x_{\text{clean}} \end{cases} \quad (14)$$

where the first constraint ensures the backdoor activates on triggered inputs, and the second maintains performance on clean inputs.

For targeted attacks, we flip specific samples to incorrect outputs:

$$\min_{\Delta\theta} \|\Delta\theta\|_2 \quad \text{s.t.} \quad f_{\theta+\Delta\theta}(x_i) = y_i^{\text{wrong}} \quad \forall i \in \mathcal{T} \quad (15)$$

where  $\mathcal{T}$  is the set of target samples.

We solve these optimization problems using SGD with gradient-based loss functions that maximize target label probabilities while minimizing perturbation magnitude via  $L_2$  regularization. To establish the lower bound on required perturbations, we optimize each attack on a single sample. In practice, attacks typically need to compromise multiple samples, which requires larger perturbations than the single-sample lower bound reported here.

**Evaluation.** We measure the minimum and maximum relative  $L_2$  parameter perturbations required for successful attacks using bfloat16 precision. Figure 7 summarizes the perturbation magnitudes for both backdoor and targeted attacks across different models.

Successful parameter poisoning requires perturbations orders of magnitude larger than numerical recomputation errors shown in Figure 5. Combined with activation-level results, this confirms that with proper precision choices, AFTUNE’s numerical tolerances cannot be exploited to inject stealthy attacks at either inference or training level. The substantial



Figure 7: Parameter poisoning attacks: parameter perturbation relative  $L_2$  norm across models.

separation between numerical errors and attack perturbations enables effective detection of meaningful tampering while accommodating legitimate floating-point variations across ML accelerators and TEE hardware.

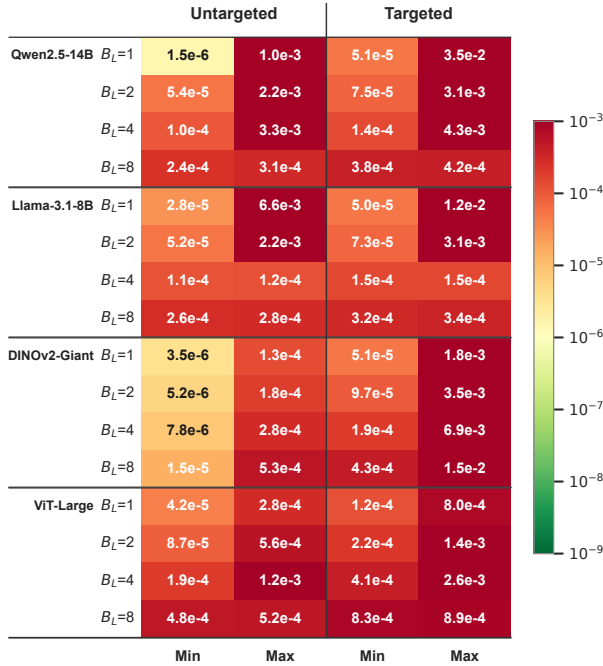


Figure 8: Adversarial example attacks: activation perturbation relative  $L_2$  norm across models and layer block sizes.

## 8 Discussion

### 8.1 Storage Management

AFTUNE’s verification storage is temporary: recorded states exist solely for audit and can be released immediately after verification completes. To further reduce storage burden, the provider can optionally adopt an incremental commit-and-prune strategy: periodically transmit hash records  $\{\mathcal{R}_{i,j}\}$  for completed training stages to the client, who specifies target

blocks for verification. The provider then deletes all non-target states before TEE provisioning, retaining only data for requested blocks. This optional strategy enables proactive storage reclamation during training rather than requiring full retention until verification completes.

For extreme storage constraints, AFTUNE supports a zero-storage strategy ( $I_C = \infty, I_A = \infty$ ) where only cryptographic hashes are recorded and transmitted during training, and the size of these commitments is negligible. Upon receiving the client’s verification request, the provider reruns the entire training from the initial checkpoint, recording states only for the requested blocks. This trades 100% additional training overhead (one full retraining pass) to eliminate temporary storage during initial training. Providers can adapt the system across a spectrum: from dense recording with minimal verification overhead to zero-storage with doubled training cost, matching their specific resource constraints, which demonstrates AFTUNE’s flexibility in balancing storage and computation costs.

### 8.2 Limitations

Our work relies on TEEs as the root of trust for verification. Like all TEE-based approaches, if the TEE itself is compromised, the security guarantees of our framework will be undermined. In addition, when clients choose to verify only a subset of blocks, the framework provides probabilistic detection guarantees rather than deterministic assurance. Although clients can employ verification strategies to defend against specific attacks with near-certain probability, malicious behavior may still have a chance of evading detection.

## 9 Conclusion

Cloud-based fine-tuning and inference create a fundamental trust gap. Clients cannot verify whether providers execute computations as contracted, and existing verification approaches fail to scale to modern LLMs due to either prohibitive overhead (ZKP-based methods) or full model encapsulation requirements (TEE-based methods). AFTUNE addresses this through block decomposition with compositional verification. By recording commitments over boundary states and enabling selective TEE-based recomputation, AFTUNE provides strong auditability while keeping primary workloads on standard accelerators with near-baseline performance.

Our evaluation demonstrates that the two-dimensional block structure offers flexibility to balance overhead, storage, and verification granularity, while map-reduce style hashing minimizes commitment costs. The sampling-based verification strategy provides probabilistic detection guarantees that compound over repeated audits. By decoupling execution from verification, AFTUNE transforms opaque AI services into accountable platforms where trust is established through verifiable evidence rather than provider claims.

## Ethical Considerations

We structure the ethical considerations by linking our stakeholder analysis to the impacts generated during the research process and publication of results.

**Stakeholder Analysis.** AFTUNE involves four primary stakeholder groups. (1) *Cloud Service Providers*: Companies offering AI fine-tuning and inference services. (2) *Clients*: Organizations outsourcing model fine-tuning and inference to cloud providers. (3) *End Users*: Individuals who interact with AI systems built on cloud-fine-tuned models. (4) *Research Community*: ML and security researchers who may build upon our framework.

**Positive Impacts.** (1) *Enhancing Trust in Cloud AI (Impact on Clients & End Users)*: AFTUNE provides clients with verifiable guarantees that contracted computations were executed faithfully, reducing the risk of silent service degradation or fraud. This indirectly benefits end users who rely on properly trained models. (2) *Promoting Accountability (Impact on Providers & Society)*: By enabling auditability, our framework incentivizes honest behavior among cloud providers, fostering a more trustworthy AI service ecosystem. (3) *Reproducibility and Open Science (Impact on Research Community)*: We open-source our implementation to enable the community to assess, audit, and improve upon our methods.

**Negative Impacts.** We are not aware of any potential harms or negative societal impacts arising from this work. Our framework is purely defensive in nature, designed to detect misbehavior rather than enable it.

**Decision to Conduct and Publish.** We initiated this research to address a practical trust problem in cloud AI services. Our work focuses on defense rather than offense. We believe sharing these results benefits the broader ecosystem by enabling clients to hold providers accountable.

## Open Science

All code and artifacts used for the experiments in this paper are available at <https://github.com/hengvt/AFTUNE>, with detailed instructions for using the framework and reproducing the experiments.

## References

- [1] How Confidential Computing lays the foundation for trusted AI | Google Cloud Blog — cloud.google.com. <https://cloud.google.com/blog/products/identity-security/how-confidential-computing-lays-the-foundation-for-trusted-ai>.
- [2] Large language model inference over confidential data using AWS Nitro Enclaves. <https://aws.amazon.com/blogs/machine-learning/large-language-model-inference-over-confidential-data-using-aws-nitro-enclaves/>.
- [3] ABBASZADEH, K., PAPPAS, C., KATZ, J., AND PAPADOPOULOS, D. Zero-knowledge proofs of training for deep neural networks. In *Proceedings of the 2024 on ACM SIGSAC Conference on Computer and Communications Security* (2024), pp. 4316–4330.
- [4] ALVES, T., AND FELTON, D. Trustzone: Integrated hardware and software security. *ARM White Paper* (2004).
- [5] ANTHROPIC. Fine-tune claude 3 haiku in amazon bedrock, July 2024.
- [6] ATENIESE, G., BURNS, R., CURTMOLA, R., HERRING, J., KISSNER, L., PETERSON, Z., AND SONG, D. Provable data possession at untrusted stores. In *Proceedings of the 14th ACM Conference on Computer and Communications Security* (New York, NY, USA, 2007), CCS '07, Association for Computing Machinery, p. 598–609.
- [7] CHE TSAI, C., PORTER, D. E., AND VIJ, M. Graphene-SGX: A practical library OS for unmodified applications on SGX. In *2017 USENIX Annual Technical Conference (USENIX ATC 17)* (Santa Clara, CA, July 2017), USENIX Association, pp. 645–658.
- [8] CHEN, H., FU, C., ROUHANI, B. D., ZHAO, J., AND KOUSHANFAR, F. Deepattest: An end-to-end attestation framework for deep neural networks. In *Proceedings of the 46th International Symposium on Computer Architecture* (2019), pp. 487–498.
- [9] CLOUD, G. Tune gemini models by using supervised fine-tuning, 2025.
- [10] CORPORATION, M. Azure openai in azure ai foundry models, 2025.
- [11] CORPORATION, O. Host llms with nvidia gpus on oci, 2025.
- [12] COSTAN, V., AND DEVADAS, S. Intel sgx explained. In *IACR Cryptology ePrint Archive* (2016), vol. 2016, p. 086.
- [13] DHAR, A., THORENS, C., LAZIER, L., AND CAVIGELLI, L. Guardain: Protecting emerging generative ai workloads on heterogeneous npu. pp. 4155–4172.
- [14] EMANI, M., FOREMAN, S., SASTRY, V., XIE, Z., RASKAR, S., ARNOLD, W., THAKUR, R., VISHWANATH, V., AND PAKKA, M. E. A comprehensive performance study of large language models on novel ai accelerators, 2023.
- [15] ET AL., A. G. The llama 3 herd of models. *arXiv preprint, arXiv:2407.21783* (2024).
- [16] FEFFER, M., SINHA, A., DENG, W. H., LIPTON, Z. C., AND HEIDARI, H. Red-teaming for generative ai: Silver bullet or security theater? In *Proceedings of the AAAI/ACM Conference on AI, Ethics, and Society* (2024), vol. 7, pp. 421–437.
- [17] HAO, M., CHEN, H., LI, H., WENG, C., ZHANG, Y., YANG, H., AND ZHANG, T. Scalable zero-knowledge proofs for non-linear functions in machine learning. In *33rd USENIX Security Symposium (USENIX Security 24)* (2024), pp. 3819–3836.
- [18] HU, E. J., SHEN, Y., WALLIS, P., ALLEN-ZHU, Z., LI, Y., WANG, S., AND CHEN, W. Lora: Low-rank adaptation of large language models. *arXiv preprint, arXiv:2106.09685* (2021).
- [19] KACHRIS, C. A survey on hardware accelerators for large language models. *Applied Sciences* 15, 2 (Jan. 2025), 586.
- [20] KUNAVAIKIL, D., STAVRAKAKIS, D., QIN, K., XING, C., BHATOTIA, P., AND VIJ, M. Gramine-tdx: A lightweight os kernel for confidential vms. In *Proceedings of the 2024 on ACM SIGSAC Conference on Computer and Communications Security* (New York, NY, USA, 2024), CCS '24, Association for Computing Machinery, p. 4598–4612.
- [21] LEE, D., KWON, M., JANG, J., AUMASSON, J.-P., BAEK, K.-H., CHOI, S., ROGERS, J., ROUSSEAU, R., AND SONG, D. Keystone: An open framework for architecting trusted execution environments. In *Proceedings of the 25th ACM International Conference on Architectural Support for Programming Languages and Operating Systems (ASPLOS)* (2020), p. 1191–1206.
- [22] LEE, J., WANG, Y., RAJAT, R., AND ANNAVARAM, M. Characterization of gpu tee overheads in distributed data parallel ml training, 2025.
- [23] LIAO, G., WANG, T., ZHANG, S., ZHANG, J., LONG, S., AND TAO, D. Verilora: Fine-tuning large language models with verifiable security via zero-knowledge proofs, 2025.

- [24] LIN, L., MU, H., ZHAI, Z., WANG, M., WANG, Y., WANG, R., GAO, J., ZHANG, Y., CHE, W., BALDWIN, T., ET AL. Against the achilles' heel: A survey on red teaming for generative models. *Journal of Artificial Intelligence Research* 82 (2025), 687–775.
- [25] MADRY, A., MAKELOV, A., SCHMIDT, L., TSIPRAS, D., AND VLADU, A. Towards deep learning models resistant to adversarial attacks, 2019.
- [26] MO, F., HADDADI, H., KATEVAS, K., MARIN, E., PERINO, D., AND KOURTELLIS, N. Ppfl: Privacy-preserving federated learning with trusted execution environments. In *Proceedings of the 19th annual international conference on mobile systems, applications, and services* (2021), pp. 94–108.
- [27] OPENAI. Introducing improvements to the fine-tuning api and expanding our custom models program. <https://openai.com/index/introducing-improvements-to-the-fine-tuning-api-and-expanding-our-custom-models-program/>, Apr. 2024.
- [28] OPENAI. Model optimization — openai api guides, 2025.
- [29] OQUAB, M., DARCEY, T., MOUTAKANNI, T., VO, H., SZAFRANIEC, M., KHALIDOV, V., FERNANDEZ, P., HAZIZA, D., MASSA, F., EL-NOUBY, A., ASSRAN, M., BALLAS, N., GALUBA, W., HOWES, R., HUANG, P.-Y., LI, S.-W., MISRA, I., RABBAT, M., SHARMA, V., SYNNAEVE, G., XU, H., JEGOU, H., MAIRAL, J., LABATUT, P., JOULIN, A., AND BOJANOWSKI, P. Dinov2: Learning robust visual features without supervision, 2024.
- [30] QU, W., SUN, Y., LIU, X., LU, T., GUO, Y., CHEN, K., AND ZHANG, J. zkqpt: An efficient non-interactive zero-knowledge proof framework for llm inference. In *34st USENIX Security Symposium (USENIX Security 25)* (2025).
- [31] QUOC, D. L., GREGOR, F., ARNAUTOV, S., KUNKEL, R., BHATOTIA, P., AND FETZER, C. securetf: A secure tensorflow framework. In *Proceedings of the 21st International Middleware Conference* (New York, NY, USA, 2020), Middleware '20, Association for Computing Machinery, p. 44–59.
- [32] RIASI, A., WANG, H., BEHNIA, R., VO, V., AND HOANG, T. Zero-knowledge ai inference with high precision. *ACM CCS* (2025).
- [33] RUSSAKOVSKY, O., DENG, J., SU, H., KRAUSE, J., SATHEESH, S., MA, S., HUANG, Z., KARPATHY, A., KHOSLA, A., BERNSTEIN, M., BERG, A. C., AND FEI-FEI, L. ImageNet Large Scale Visual Recognition Challenge. *International Journal of Computer Vision (IJCV)* 115, 3 (2015), 211–252.
- [34] SERVICES, A. W. Amazon bedrock — build generative ai applications with foundation models, 2025.
- [35] SHACHAM, H., AND WATERS, B. Compact proofs of retrievability. *J. Cryptol.* 26, 3 (July 2013), 442–483.
- [36] SILVANO, C., IELMINI, D., FERRANDI, F., FIORIN, L., CURZEL, S., BENINI, L., CONTI, F., GAROFALO, A., ZAMBELLI, C., CALORE, E., SCHIFANO, S., PALESI, M., ASCIA, G., PATTI, D., PETRA, N., DE CARO, D., LAVAGNO, L., URSO, T., CARDELLINI, V., CARDARILLI, G. C., BIRKE, R., AND PERRI, S. A survey on deep learning hardware accelerators for heterogeneous hpc platforms. *ACM Comput. Surv.* 57, 11 (June 2025).
- [37] STEIAKAKIS, N.-A., AND VASILIAKIS, G. Trusted yet flexible: High-level runtimes for secure ml inference in tees. *Journal of Cybersecurity and Privacy* 6, 1 (2026).
- [38] SUN, H., LI, J., AND ZHANG, H. zkllm: Zero knowledge proofs for large language models. In *Proceedings of the 2024 on ACM SIGSAC Conference on Computer and Communications Security* (2024), pp. 4405–4419.
- [39] SUN, Y., LI, Y., ZHANG, Y., JIN, Y., AND ZHANG, H. Svip: Towards verifiable inference of open-source large language models. *arXiv preprint arXiv:2410.22307* (2025).
- [40] TAN, Y., TAN, C., MI, Z., AND CHEN, H. Pipellm: Fast and confidential large language model services with speculative pipelined encryption. In *Proceedings of the 30th ACM International Conference on Architectural Support for Programming Languages and Operating Systems, Volume 1* (New York, NY, USA, 2025), ASPLOS '25, Association for Computing Machinery, p. 843–857.
- [41] TANG, D., ZHOU, J., HU, J., LI, S., ZHENG, H., PEI, Z., WANG, H., AND ZHANG, X. H2:towards efficient large-scale llm training on hyper-heterogeneous cluster over 1,000 chips, 2025.
- [42] WU, B., XU, C., DAI, X., WAN, A., ZHANG, P., YAN, Z., TOMIZUKA, M., GONZALEZ, J., KEUTZER, K., AND VAJDA, P. Visual transformers: Token-based image representation and processing for computer vision, 2020.
- [43] XIE, T., LU, T., FANG, Z., WANG, S., ZHANG, Z., JIA, Y., SONG, D., AND ZHANG, J. zkpytorch: A hierarchical optimized compiler for zero-knowledge machine learning. *Cryptology ePrint Archive* (2025).
- [44] XU, J., WEI, T., HOU, B., ORZECZOWSKI, P., YANG, S., JIN, R., PAULBECK, R., WAGENAAR, J., DEMIRIS, G., AND SHEN, L. Mentalchat16k: A benchmark dataset for conversational mental health assistance. *arXiv preprint arXiv:2503.13509* (2025).
- [45] YAN, R., JIANG, Y., NIE, X., FU, F., CUI, B., AND YUAN, B. Hex-yscale: Accommodating large language model training over heterogeneous environment, 2025.
- [46] YANG, A., YANG, B., ZHANG, B., HUI, B., ZHENG, B., YU, B., LI, C., LIU, D., HUANG, F., WEI, H., LIN, H., YANG, J., TU, J., ZHANG, J., YANG, J., YANG, J., ZHOU, J., LIN, J., DANG, K., LU, K., BAO, K., YANG, K., YU, L., LI, M., XUE, M., ZHANG, P., ZHU, Q., MEN, R., LIN, R., LI, T., TANG, T., XIA, T., REN, X., REN, X., FAN, Y., SU, Y., ZHANG, Y., WAN, Y., LIU, Y., CUI, Z., ZHANG, Z., AND QIU, Z. Qwen2.5 technical report. *arXiv preprint, arXiv:2412.15115* (2025).
- [47] ZHANG, E., PAL, A., POTTI, A., AND GOLDBLUM, M. vtune: Verifiable fine-tuning for llms through backdooring. *arXiv preprint arXiv:2411.06611* (2024).
- [48] ZHANG, X., LI, F., ZHANG, Z., LI, Q., WANG, C., AND WU, J. Enabling execution assurance of federated learning at untrusted participants. In *IEEE INFOCOM 2020-IEEE Conference on Computer Communications* (2020), IEEE, pp. 1877–1886.
- [49] ZHAO, L., JIANG, J., FENG, B., WANG, Q., SHEN, C., AND LI, Q. Sear: Secure and efficient aggregation for byzantine-robust federated learning. *IEEE Transactions on Dependable and Secure Computing* 19, 5 (2021), 3329–3342.

## A Possible Attacks

Below we outline several classes of provider misbehavior that the visibility gap makes possible. In all these cases, the attacks can be profitable for the provider, hard to catch with final accuracy or black-box testing alone, and leave the client with no verifiable record of what actually happened during training or inference.

### A.1 Attacks in Training

#### A.1.1 Under-training

An untrusted provider may try to cut training cost while still charging for the full job. The provider might silently reduce epochs, truncate batches, skip parts of the dataset, or drift from the agreed hyperparameter schedule, then bill as if the contracted training had been run in full. For example, a client who paid for 3 epochs over 100K samples might receive a model trained for 1 epoch on 50K samples, good enough to pass rough checks but weaker on held-out or long-tail data.

#### A.1.2 Model substitution

Instead of the contracted base model, the provider may use a weaker checkpoint from the start or switch to a cheaper model (e.g., a smaller or distilled one) partway through training. The client pays for fine-tuning from a strong base but has no way to verify that the delivered model was actually trained from that base.

#### A.1.3 Backdoors and poisoning

A compromised or malicious provider could inject backdoors or other latent behaviors during training. These pass normal quality checks but trigger on specific inputs (e.g., certain phrases or embedded triggers), so the model misbehaves only when those conditions are met. For example, a malicious employee at the provider could add a backdoor to the training set to steer the LLM’s behavior, then remove that backdoor from the training set after training is done. As long as the trigger remains unknown, this behavior cannot be detected or verified by the client.

### A.2 Attacks in Inference

#### A.2.1 Serving the wrong model

At serving time, the provider might run a cheaper model than the one the client believes is deployed. For instance, serving the base model or a distilled copy instead of the client’s fine-tuned model, while claiming to serve the latter.

#### A.2.2 Fabricated or manipulated responses

The provider might skip running the model altogether for some requests: return cached or templated responses for repeated or similar queries to save compute. A malicious or compromised provider may also directly manipulate returned results, for example, deliberately altering or injecting responses to steer the client’s downstream decisions, spread misinformation, or exfiltrate or poison data.

## B Algorithm to Verify One Training Block

---

### Algorithm 1 Verify Block Cell

---

**Require:** Layer block index  $i$ , step block index  $j$ , recorded hash set  $\mathcal{R}_{i,j}$ , parameters  $\{\theta_{l,j:B_S}\}_{l \in \text{LB}_i}$ , optimizer states  $\{s_{l,j:B_S}\}_{l \in \text{LB}_i}$ , boundary states, and numerical tolerance  $\tau$

**Ensure:** Verification result: PASS or FAIL

- 1: **Step 1: Load model state in TEE**
- 2: Load parameters and optimizer states for layers in  $\text{LB}_i$  at step  $j \cdot B_S$  into TEE memory
- 3: **Step 2: Verify target block cell**
- 4: **for** each step  $t \in \text{SB}_j$  **do**
- 5:   **Forward pass:**
- 6:    $\hat{x}_{l_{\text{in}},t}, \hat{y}_{l_{\text{out}},t} \leftarrow \text{ForwardBlock}(\text{LB}_i, x_{l_{\text{in}},t-1,t})$
- 7:   **Hash verification (integrity):**
- 8:   **if**  $H(\hat{x}_{l_{\text{in}},t}) \neq H(x_{l_{\text{in}},t}) \in \mathcal{R}_{i,j}$  **then**
- 9:     **return** FAIL
- 10:   **end if**
- 11:   **if**  $H(\hat{y}_{l_{\text{out}},t}) \neq H(y_{l_{\text{out}},t}) \in \mathcal{R}_{i,j}$  **then**
- 12:     **return** FAIL
- 13:   **end if**
- 14:   **Numerical verification:**
- 15:   **if**  $\|\hat{y}_{l_{\text{out}},t} - y_{l_{\text{out}},t}\| / \|y_{l_{\text{out}},t}\| > \tau$  **then**
- 16:     **return** FAIL
- 17:   **end if**
- 18:   **Backward pass and gradient verification:**
- 19:    $\hat{\nabla}x_{l_{\text{in}},t}, \hat{\nabla}y_{l_{\text{out}},t} \leftarrow \text{BackwardBlock}(\text{LB}_i, \nabla y_{l_{\text{out}},t+1,t})$
- 20:   Verify hashes and numerical correctness for gradients (similar to forward pass)
- 21:   **Parameter update and verification:**
- 22:    $\hat{\theta}_{t+1}, \hat{s}_{t+1} \leftarrow \text{OptimizerStep}(\hat{\theta}_t, \hat{s}_t, \hat{\nabla}\theta_t)$
- 23:   Verify hashes and numerical correctness for updated parameters and optimizer states
- 24: **end for**
- 25: **return** PASS

---

## C Verification Chain and Trust Anchors

A key question emerges: as described in Section 5.4, verification inside the TEE depends on hash matching, but the hashes themselves are computed by the service provider during train-

ing. If the provider is untrusted, how can its hashes serve as a basis for trust?

In traditional data storage auditing, hashes are computed by the client before uploading data, so the client can directly trust the hash values. In our framework, however, hashes are computed by the cloud provider during training. The correctness of these hashes is instead guaranteed through a verification chain formed by neighboring blocks.

Specifically, for any block  $B_{i,j}$ , the hash values used for verification derive their correctness from adjacent blocks:  $B_{i-1,j}$  provides the correctness guarantee of inputs,  $B_{i+1,j}$  provides the correctness guarantee of gradients, and  $B_{i,j-1}$  provides the correctness guarantee of parameters, following the model computation procedure. The correctness of these neighboring blocks can be similarly traced back to their own neighbors. Ultimately, all blocks form a verification chain, where each block serves to validate its adjacent blocks, and the entire chain is anchored to trusted roots: the initial model weights, and the client-provided inputs and labels. Figure 9 illustrates this trust propagation.

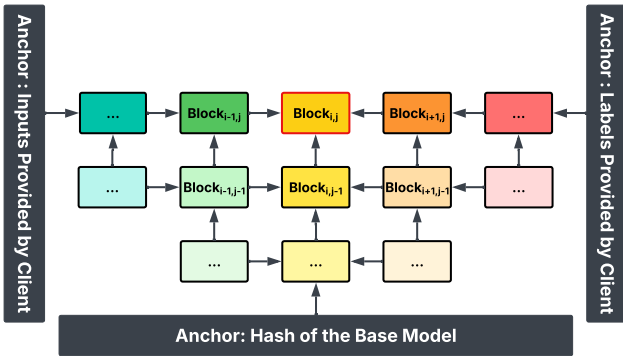


Figure 9: Trust propagation to block  $B_{i,j}$ : correctness is derived from the anchor through neighboring blocks. Outgoing trust flows are omitted for clarity. Note that commitments of all blocks within each row must be submitted together, establishing mutual dependencies among them.

We require the cloud provider to publicly release the hash commitment of the base model before any fine-tuning contract is established. This serves as the parameter anchor without revealing actual model weights. At this point, since no specific fine-tuning agreement exists, the provider cannot preemptively attack the base model for a particular client. The inputs and labels are provided by the client, who can compute their hashes independently. Thus, for any block, its hash correctness is ultimately linked through other blocks and anchored to these established trust roots. We recap that for each block, at the time when an attack could be performed, the attacker cannot know whether this block will later be selected for verification.

One might ask: what happens if an attacker successfully

compromises a block that happens not to be verified, as discussed in Section 5.7? If such a block escapes verification, the damage to that specific block has already occurred. However, since this block also submits its hash commitments, which remain immutable once submitted, these commitments become new trust anchors for verifying neighboring blocks, and any new attack on other blocks would still be detected. Consequently, the verification of other blocks remains unaffected. Therefore, our framework provides the same security guarantees as traditional data storage auditing for the overall training process.

## D Sparse Checkpointing Trade-offs

Table 4 shows how different checkpoint interval configurations affect training overhead, storage cost, and verification time. We fix  $B_L = 4, B_S = 8$  and vary  $I_C$ .

Table 4: Trade-offs of different checkpoint intervals on Llama-3.1-8B. Baseline is  $I_C = 1$ .

$I_C$	Train Time (s)	Prep Time (s)	Storage (GB)	Storage Ratio
1	82.9	-	355.6	1.00×
2	79.4	7.3	235.9	0.66×
4	77.2	9.4	176.1	0.50×
8	76.1	15.1	146.2	0.41×
16	75.6	29.8	131.2	0.37×

Increasing checkpoint intervals reduces both training overhead (fewer checkpoint saves) and storage requirements, but increases preparation time due to longer recomputation distances. Beyond  $I_C = 8$ , further increases yield diminishing returns in training time reduction while preparation time continues to grow significantly.

When  $I_C$  is sufficiently large, storage is dominated by activations and gradients rather than checkpoints. One might consider applying  $I_A > 1$  (sparse layer-wise boundary recording) to further reduce storage. However, this is more costly for training block verification due to bidirectional dependency: verifying any block requires both its input activation (from forward) and output gradient (from backward), necessitating full recomputation of  $2 \times I_A + 1$  consecutive blocks including forward, backward, and parameter updates. This substantially increases preparation time as  $I_A$  grows. Therefore, we fix  $I_A = 1$  for training verification.

## E Optimizer Comparison

Table 5 compares AdamW and SGD optimizers across different models using the second configuration from Table 1. We measure storage cost, training time, training overhead, block preparation time, and TEE verification time per 2048 samples.

Qwen2.5-14B cannot be trained with AdamW due to GPU memory constraints.

Table 5: Optimizer comparison: storage, training time, overhead, and verification metrics per 2048 samples.

Model	Metric	SGD	AdamW
Llama-3.1-8B	Train Time (s)	76.1	114.5
	Overhead	21%	33%
	Storage (GB)	146.2	206.6
	Prep Time (s)	15.1	22.4
	Verify Time (s)	48.2	83.0
DINOv2-Giant	Train Time (s)	34.8	48.5
	Overhead	44%	81%
	Storage (GB)	19.1	27.7
	Prep Time (s)	10.4	14.5
	Verify Time (s)	25.6	32.1
ViT-Large	Train Time (s)	8.9	12.1
	Overhead	31%	66%
	Storage (GB)	2.9	5.2
	Prep Time (s)	4.6	7.1
	Verify Time (s)	15.3	20.8

The results reveal systematic differences between optimizers across all metrics. AdamW’s optimizer state requires twice the parameter size (storing both momentum and variance terms). Training overhead with AdamW is 10-35 percentage points higher than SGD due to additional time required to save and hash larger optimizer states at step block boundaries. Preparation and verification times are also higher for AdamW due to increased recomputation and verification costs for optimizer state updates.

## F Chunk Size and Hash Function Analysis

We evaluate the impact of chunk size and hash function choice on hash computation time, as described in Section 5.3. The chunk size affects both training-time hash computation (during forward/backward passes) and verification-time hash computation (during TEE recomputation).

Figure 10 shows the relationship between chunk size and hash computation time for Llama-3.1-8B. We vary chunk size from 1024 to 10240 elements and measure both training hash time and verification hash time per block cell. We compare BLAKE3 and SHA-256 hash functions to demonstrate their performance characteristics.

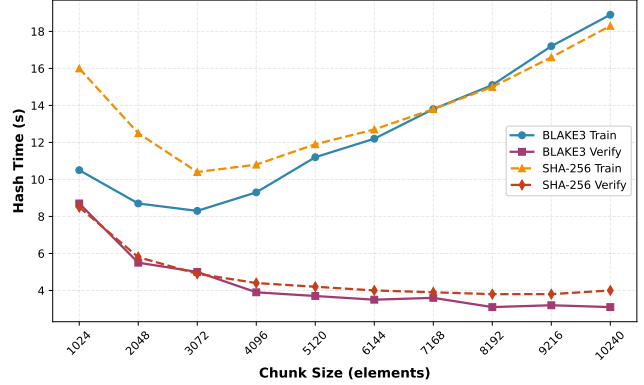


Figure 10: Impact of chunk size on hash computation time for Llama-3.1-8B. Different optimal chunk sizes emerge for GPU-based training hashing vs. CPU-based verification hashing.

The results reveal distinct performance patterns for GPU and CPU hashing. For GPU-based training hashing on Llama-3.1-8B, an optimal chunk size around 3072 elements balances parallelism against per-thread computation overhead. Both BLAKE3 and SHA-256 achieve minimal latency at this point, with performance degrading for larger chunks due to insufficient parallelism. In contrast, CPU-based verification hashing shows monotonically improving performance with larger chunk sizes, as the limited parallelism benefits from reduced per-chunk overhead.

Hash function choice also exhibits platform-dependent behavior. On the GPU, BLAKE3 outperforms SHA-256 for chunk sizes below 8192 elements, but performance converges for larger chunks. This behavior stems from BLAKE3’s tree-based internal structure: our implementation assigns each chunk to a separate GPU thread, and BLAKE3’s tree construction performs multiple memory copy operations to manage intermediate hash states within each chunk. As chunk size increases, the number of internal memory operations within each chunk grows proportionally, amplifying the memory latency overhead. GPU memory latency is significantly higher than CPU cache latency, making BLAKE3’s memory-intensive tree construction increasingly expensive for larger chunks. On the CPU, BLAKE3 consistently outperforms SHA-256 across all chunk sizes, as the CPU’s cache hierarchy effectively hides memory latency.